This article has been accepted for publication in a future issue of this journal, but has not been fully edited. Content may change prior to final publication. Citation information: DOI 10.1109/LSP.2017.2670026, IEEE Signal Processing Letters

Multiscale Sampling Based Texture Image Classification

Yongsheng Dong, Jinwang Feng, Lingfei Liang, Lintao Zheng, and Qingtao Wu

***Abstract*—The widely used energy features extracted from the wavelet domain can effectively represent the common image textures. However, they are not robust to the rotated textures. In this paper, we propose a multiscale rotation-invariant representation (MRIR) of textures by using multiscale sampling. Particularly, a multiscale wavelet transform is used to decompose the magnitude pattern (MP) mapping of a texture. Furthermore, the sign pattern (SP) mapping of a texture is used as a step function, which is further sampled and used to fit the wavelet subbands of the MP mapping for computing the sampled directional mean vectors (SDMVs) of the subbands. Moreover, we construct frequency vectors (FVs) of those SP mappings for capturing the structural information of textures. Finally, we can obtain the MRIR vector of an image texture by concatenating those SDMVs and FVs for texture classification. The comprehensive experimental results demonstrate that our proposed approach outperforms six representative texture classification methods.**

***Keywords*—Texture representation, wavelet transform, rotation invariance, energy feature, image classification.**

I. Introduction

IMAGE analysis is an important area of computer vision and pattern recognition. Due to that texture is a primary characteristic of images, a variety of texture representation methods have been proposed in last three decades, which can be roughly categorized into spacial domain-based [1]-[7] and transform-based [8]-[13] methods.

The spacial domain based method mainly uses the local information of textures to construct image features [14]-[18]. Ojala et al. [19] used the local binary pattern (LBP) computed by encoding the differences between the center pixel and its neighbors in a patch as texton for texture classification. Guo et al. [20] gave a completed LBP (CLBP) method by combining the sign and magnitude of neighboring differences and the center pixels for texture representation. Qi et al. [21] used rotation-invariant co-occurrence LBP for texture classification. Although the above methods considered the multiscale information by changing the scale of a local neighborhood, they neglect the directional information of textures.

Y. Dong, J. Feng, L. Liang, L. Zheng, and Q. Wu are with Information Engineering College, Henan University of Science and Technology, Luoyang 471023, Henan, P. R. China.

This work was supported in part by the National Natural Science Foundation of China under Grants U1604153, in part by the China Scholarship Council under Grant 201608410233, in part by the International Science and Technology Cooperation Project of Henan Province under Grant 162102410021, and in part by the Program for Innovative Research Team (in Science and Technology) in University of Henan Province under Grant 14IRTSTHN021.

In the transform-based methods, directional multiscale tranforms, such as wavelets [22]-[25], shearlets [26], and contourlets [27]-[29], are widely utilized for representing an image texture. Generally speaking, statistical models are employed for modeling the transformed coefficients to construct effective texture descriptors. The usually used models include bit-plane model [16], local energy histograms [22], Poisson mixture model [27], linear regression model [26] and so on. Besides, nonnegative matrix factorization can be used for constructing compact texture representation [23], [30]. Although those transform-based methods effectively represent the common image texture, they are not robust to the rotated textures.

Motivated by the above problems, we in this paper propose a multiscale rotation-invariant representation (MRIR) of textures by using multiscale sampling. Particularly, a multiscale wavelet transform is used to decompose the magnitude pattern (MP) mapping of a texture. We further compute the sign pattern (SP) mapping of a texture, and sample it for matching the wavelet subbands of the MP mappings to compute the sampled directional mean vectors (SDMVs) of each wavelet subband. In addition, frequency vectors (FVs) of those SP mappings are also constructed for capturing the structural information of textures. Furthermore, the texture information at a given scale can be described by three SDMVs and a FV. Therefore, a texture can be represented by a concatenation of the features at all scales consisting of the above SDMVs and FVs.

Three contributions are made in this paper. First, we propose a multiscale sampling scheme to construct a matching template. As a two-dimensional step function, the matching template can be used to compute the component energies of each wavelet subband, which can capture more information than the traditional energy extraction method. Second, we build a multiscale rotation-invariant representation to describe textures, which can be effectively used for performing the classification of the rotational textures. Finally, we construct a rotated Brodatz dataset for evaluating our proposed method according to the original Brodatz database. Experimental results on Brodatz, KTH-TIPS2-a, and Outex databases reveal that our proposed method outperforms the representative methods.

The remainder of this paper is organized as follows. Section II introduces the proposed multiscale rotation-invariant texture representation framework. Experimental results in Section III demonstrate the effectiveness of our proposed method. Finally, we briefly conclude in Section IV.

II. Multiscale Rotation-Invariant Texture Representation Framework

Rotation invariance is an important characteristic in image analysis. To alleviate the limitation of transform-based method

This article has been accepted for publication in a future issue of this journal, but has not been fully edited. Content may change prior to final publication. Citation information: DOI 10.1109/LSP.2017.2670026, IEEE Signal Processing Letters

in terms of image rotation, we first perform a rotation-invariant processing to a texture image, followed by a wavelet transform. We then construct the MRIR feature of a texture image.

A. Multiscale Sampling

1) Wavelet Based Multiscale Decomposition of Magnitude Pattern Mapping: For a pixel in the given texture image, its magnitude pattern (MP) is defined as

$$MP = \sum_{i=1}^{P} |x_i - x_c|. \tag{1}$$

where x_c is the current pixel and x_i is its i-th neighbor of the P ones which are equally distributed on a circle with radius R. The neighbors not located in the image grid can be computed by bilinear interpolation. According to equation (1), values in the MP mapping are rotation-invariant, the reason is that a pixel is described by the sum of magnitudes of differences between the pixel and its neighbors, which is not relevant to the neighboring positions and gray levels [19].

To use the multiscale information of texture images, multiscale wavelet transform with the Daubechies 8 (db8) filter bank is thus adopted to decompose the two-dimensional MP mapping. For a L-scale wavelet decomposition to the MP mapping, $3 * L$ high-pass subbands $\{W_{ij}\}_{i=1,\ldots,L,j=1,2,3}$ and a low-pass subband W_0 can be obtained. It is obvious that we can get $3 * L + 1$ subbands of the MP mapping. Note that those obtained subbands are rotation-invariant in terms of image rotations

2) Sampling of Sign Pattern Mapping: For the pixel, its sign pattern (SP) is defined as

$$SP = \sum_{i=1}^{P} s(x_i - x_c), \tag{2}$$

where $s(x)$ is a sign function that is defined as

$$s(x) = \begin{cases} 1, & x \geq 0 \\ 0, & x < 0 \end{cases}. \tag{3}$$

Similarly, values in the SP mapping are also rotation-invariant according to equation (2) [19], [20].

Note that pixels of a texture image are represented by values in the MP and SP mappings after the rotation-invariant processing. Obviously, the magnitude information of pixels is incorporated in the MP mapping. While the SP mapping contained the sign information of pixels, which composes of discrete values and has $P + 1$ pattern classes.

In order to use the SP mapping as a step function to split coefficients in a subband at different scales, the downsampling process corresponding to wavelet decomposition is thus done for the SP mapping to generate L distributions of values of the step function. The i-th scale distribution is

$$T^i = T^{i-1}(1:2:end, 1:2:end), i = 1, \ldots, L, \tag{4}$$

where T^0 is the SP mapping and $T^{i-1}(1:2:end, 1:2:end)$ is a down-sampling process of every other line and very other column. For clarity, the $L+1$ step function value distributions are denoted as $\{T^i\}_{i=0,\ldots,L}$.

B. Multiscale Rotation-Invariant Representation

It is obvious that a subband at the i-th sclae can be split into $P + 1$ partitions by the step function value distribution T^i. For clarity, all partitions of those subbands are denoted as $\{S_{ij}^k\}_{i=1,\ldots,L,j=1,2,3}^{k=1,\ldots,P+1}$. Here S_{ij}^k is the k-th partition of the j-th $M \times N$ subband at the i-th scale, which is defined as

$$S_{ij}^k = \bigcup_{\substack{x=1,\ldots,M \\ y=1,\ldots,N \\ T^i(x,y)=k}} W_{ij}(x,y), k \in [0, P] \tag{5}$$

where $W_{ij}(x,y)$ and $T^i(x,y)$ are the subband coefficient and the step function value at the position (x,y) of W_{ij} and T^i respectively. Its mean value, e_{ij}^k, is defined as

$$e_{ij}^k = \frac{1}{|S_{ij}^k|} \sum_{\tau=1}^{|S_{ij}^k|} |z_\tau|. \tag{6}$$

Note that the e_{ij}^k can be seen as the component energy of the wavelet subband S_{ij}^k. In this paper, the value of e_{ij}^k is used as the k-th element of the sampled directional mean vector (SDMV). Thus, the SDMV of the j-th subband at the i-th scale can be represented by

$$SDMV_{ij} = (e_{ij}^0, e_{ij}^1, \ldots, e_{ij}^P). \tag{7}$$

That is to say, the SDMV consisting of component energies of the wavelet subband. This is different from the commonly used energy feature extraction method in which only a energy feature is extracted to represent a wavelet subband. So our proposed SDMV can capture more information of a given wavelet subband.

In order to enhance the discrimination and rotation-invariance of the i-th scale SDMV, a frequency vector (FV), FV^i, of the sampled $M \times N$ SP mapping, T^i, is also constructed. Its k-th element, B_k, is

$$B_k = \sum_{x=1}^{M} \sum_{y=1}^{N} f(T^i(x,y) - k), k \in [0, P] \tag{8}$$

where $f(a) = 1$ when $a = 0$, otherwise $f(a) = 0$.

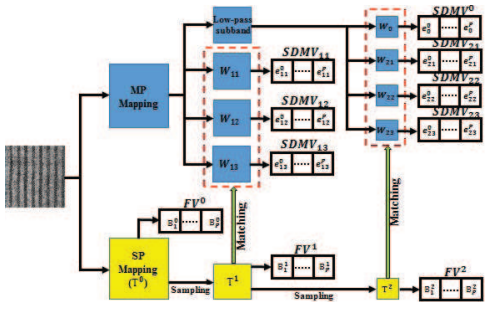

Fig. 1. The extraction process of our proposed MRIR consisting of the sampled directional mean vectors (SDMVs) and the frequency vectors (FVs) with $L = 2$.

Fig. 1 shows the extraction process of our proposed MRIR consisting of SDMVs and FVs. For clarity, we only show

the two scale decomposition and sampling. As we can see from Fig. 1, a texture is first decomposed into the MP and SP mappings, then wavelet transform and sampling are done for them respectively. Furthermore, SDMVs of subbands are built by using those matching templates. Finally, FVs of those SP mappings are also extracted at different scales.

Thus, the rotation-invariant representation (RIR) of the l-th scale is defined as

$$RIR^i = (SDMV^i, FV^i), \tag{9}$$

where $SDMV^i = (SDMV_{i1}, SDMV_{i2}, SDMV_{i3})$ is a collection of SDMVs of subbands at the i-th scale. For W_0, its SDMV is also useful in capturing texture information [22], which is computed and denoted as $SDMV^0$ for uniformity. In order to avoid information redundancy, the frequency vector of the SP mapping denoted as FV^0 is constructed for W_0. Thus the low-pass RIR feature is

$$RIR^0 = (SDMV^0, FV^0). \tag{10}$$

Finally, a multiscale rotation-invariant representation (M-RIR) contained all subbands and texture structures at different scales is constructed by

$$MRIR = (RIR^0, RIR^1, \ldots, RIR^L). \tag{11}$$

Once we obtain the MRIRs of all texture samples, we can use the minimum distance classifier for classification, which will be described in detail in the following section.

III. Experiments

In this section, comprehensive experiments are conducted to demonstrate the effectiveness of our proposed texture representation method. In addition, average classification accurate rate (ACAR) of ten random splits of the training and testing samples of a dataset is used as its final experimental result.

A. Dissimilarity Measurement

In this paper, nearest neighbor classifier with Chi-square distance is selected for dissimilarity measurement. For $MRIR^1$ and $MRIR^2$, the Chi-square distance is

$$D(MRIR^1, MRIR^2) = \sum_{i=1}^{A} \frac{(B_i^1 - B_i^2)^2}{B_i^1 + B_i^2}, \tag{12}$$

where B_i^1 and B_i^2 are the i-th element of A ones in the two features respectively. In experimental phase, a test sample is classified to the class to which the training sample obtaining the minimum distance belongs.

B. Datasets

1) Brodatz-based Texture Datasets: Considering Brodatz album is a widely-used benchmark, we first test our proposed method on three texture datasets obtained from the original Brodatz texture dataset. These three datasets was used in [26]. For simplicity, they are denoted as Set-1, Set-2, and Set-3 respectively. Forty images are contained in Set-1. Set-2 composes of forty images in Set-1 and another twenty images. The largest Set-3 is the whole Brodatz database. The 512×512 centre patch of each image in the three datasets is firstly cropped. Subsequently, each patch is divided into 16 128×128 samples.

To verify its robustness on the rotated textures, we further construct three rotated Brodatz texture datasets by respectively rotating three original Brodatz texture datasets in terms of nine angles ($0°, 5°, 10°, 15°, 30°, 45°, 60°, 75°$, and $90°$). For clarity, we denote these three new datasets as Set-4, Set-5, and Set-6. And then the 320×320 centre patches of those rotated images are cropped. Finally, each patch is divided into 16 80×80 samples. In the experimental phase, for those Brodatz-based texture datasets, half samples randomly selected from each class are used for training and the rest is used for testing.

2) The other Datasets: The KTH-TIPS2-a dataset [1], [4], [18] composes of 11 texture classes; each class contains four samples. According to the experimental protocol utilized by previous studies, we also use one sample of each class as training set and the rest is used for testing set.

The Outex_TC_00012 suite [1], [4] of Outex, denoted as Outex in the following, consists of 24 texture classes and 9120 texture samples under different rotation angles ($0°, 5°, 10°, 15°, 30°, 45°, 60°, 75°$, and $90°$) and illumination conditions (inca, t184, and horizon). In the experimental stage, the training set contains samples with rotation angle $0°$, and each test set has the other different rotation angles.

C. Parameter Estimation

In our method, two parameters, the wavelet decomposition scale L and the number of neighbors P around a pixel, need to be estimated. Here, two estimation experiments with different training samples, Ntr, are conducted to get the optimal values of L and P on Set-1 and Set-4 respectively. Relationships between ACARs and Ntr on the two datasets are shown in Fig. 2. The first row shows the experimental results with different L values when P=8. Obviously, the best ACARs can be achieved when L=1. The second row gives the experimental results with different P values when L=1. In this conditions, the best ACARs can be obtained when P=10. Thus L=1 and P=10 are used to our method in the absence of other instructions.

D. Experimental Results on Brodatz Database

To test the discrimination of our proposed method on original Brodatz database, experiments on Set-1, Set-2, and Set-3 are performed separately. ACARs of the representative methods LRS-MD [26], PMC-BC [27], CLBP [20], MLEP [18], Cov-LBPD [4], scLBP [1] and our proposed MRIR are given in Table I. From Table I, it can be seen that MRIR is marginally outperforms the six methods on the three original Brodatz datasets, and the standard deviations of MRIR are a few less than the six methods on the three datasets respectively. In addition, ACARs of partial features (denoted as MRIR-FV and MRIR-SDMV) of MRIR show that the discrimination is enhanced by concatenating them together. Thus, our MRIR feature can describe image textures well in dealing with those un-rotated texture images. In the next subsection, experiments

This article has been accepted for publication in a future issue of this journal, but has not been fully edited. Content may change prior to final publication. Citation information: DOI 10.1109/LSP.2017.2670026, IEEE Signal Processing Letters

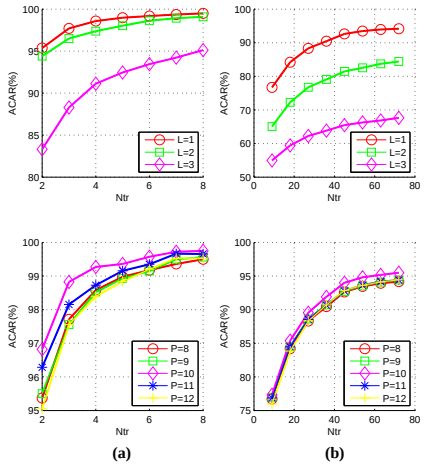

Fig. 2. Relationships between ACARs and Ntr on Set-1 and Set-4. (a) Experimental results on Set-1, (b) experimental results on Set-4.

are done to evaluate our MRIR feature for classifying rotated texture images.

TABLE I. AVERAGE CLASSIFICATION ACCURACY RATES (ACARS, %) OF THE COMPARATIVE METHODS LRS-MD, PMC-BC, CLBP, MLEP, COV-LBPD, SCLBP AND OUR MRIR ON SET-1, SET-2, AND SET-3.

Methods	Set-1	Set-2	Set-3
LRS-MD [26]	99.66±0.54	99.04±0.60	88.38±1.28
PMC-BC [27]	98.13±0.85	98.42±0.59	86.01±1.93
CLBP [20]	97.41±0.99	95.90±0.94	76.90±1.73
MLEP [18]	97.73±0.75	95.97±0.82	76.92±1.62
Cov-LBPD [4]	98.01±0.84	96.34±0.42	78.35±1.43
scLBP [1]	99.29±0.73	98.31±0.58	83.34±1.53
MRIR-FV	97.01±0.92	93.50±0.14	75.20±1.87
MRIR-SDMV	99.11±0.49	97.92±0.04	79.00±1.33
MRIR	**99.75±0.32**	**99.52±0.28**	**88.60±1.23**

To further evaluate the discrimination of MRIR in dealing with rotated texture images, another three experiments on Set-4, Set-5, and Set-6 are done. ACARs of the comparative methods and MRIR are shown in Table II. From Table II, it is obvious that ACARs of MRIR outperform the six representative methods. The better experimental results 94.50% on Set-4, 91.78% on Set-5, and 69.85% on Set-6 are obtained by our MRIR. The standard deviations of MRIR are also less than the three methods except for standard deviations of CLBP on Set-5 and Set-6. Experimental results on those rotated datasets demonstrate that rotation invariance is incorporated in our MRIR feature and the discrimination of the wavelet based feature is enhanced.

From comparisons between Table I and Table II, it can be seen that ACARs of LRS-MD and PMC-BC deteriorate rapidly, which reveals that the transform-based method is sensitive to image rotations. For CLBP, MLEP, Cov-LBPD, and scLBP, their experimental results on the two class datasets have a small change, which suggests that the spacial domain based method is rotation-invariant. Apparently, our MRIR can get the better classification results on the two class datasets, the reason is that the rotation invariance is contained in our MRIR.

TABLE II. AVERAGE CLASSIFICATION ACCURACY RATES (ACARS, %) OF THE COMPARATIVE METHODS LRS-MD, PMC-BC, CLBP, MLEP, COV-LBPD, SCLBP AND OUR PROPOSED MRIR ON SET-4, SET-5, AND SET-6.

Methods	Set-4	Set-5	Set-6
LRS-MD [26]	64.82±2.29	58.11±2.61	37.59±2.02
PMC-BC [27]	74.51±0.79	71.28±0.94	48.32±1.23
CLBP [20]	81.77±0.99	76.49±0.82	52.71±0.64
MLEP [18]	83.96±0.71	78.53±0.95	54.72±1.34
Cov-LBPD [4]	85.53±0.64	80.96±1.43	59.21±1.79
scLBP [1]	91.62±0.63	89.33±1.00	65.75±1.31
MRIR-FV	89.41±0.69	87.90±0.94	58.40±1.13
MRIR-SDMV	90.77±0.59	89.01±1.01	63.32±1.30
MRIR	**94.50±0.59**	**91.78±0.89**	**69.85±1.11**

E. Experimental Results on The Other Datasets

In order to extensively compare our MRIR with those representative methods, experiments on KTH-TIPS2-a and Outex datasets are conducted. Experimental results of the representative methods and our MRIRs are shown in Table III. Obviously, results of our MRIR on the two challenging datasets marginally outperform the representative methods according to Table III. Those experimental results further demonstrate the effectiveness of our proposed method in dealing with texture image classification under rotation condition.

TABLE III. EXPERIMENTAL RESULTS (%) OF THE COMPARATIVE METHODS LRS-MD, PMC-BC, CLBP, MLEP, COV-LBPD, SCLBP AND OUR PROPOSED MRIR ON KTH-TIPS2-A AND OUTEX.

Methods	KTH-TIPS2-a	Outex
LRS-MD [26]	58.39	51.33
PMC-BC [27]	62.74	59.06
CLBP [20]	66.58	95.37
MLEP [18]	75.57	97.32
Cov-LBPD [4]	74.86	96.70
scLBP [1]	78.39	98.15
MRIR-FV	63.75	92.03
MRIR-SDMV	72.81	97.54
MRIR	**78.52**	**98.28**

In summary, experimental results on the three widely used Brodatz, KTH-TIPS2-a, and Outex databases reveal that our proposed MRIR method outperforms the six representative methods.

IV. CONCLUSION

In this paper, we investigate the rotation-invariant texture representation problem, and propose a multiscale rotation-invariant representation of textures based on multiscale sampling for classification. To this end, we first construct the matching template to capture component energies of each wavelet subband of magnitude pattern (MP) mapping of a texture. These component energies are further used for building the sampled directional mean vector(SDMV). Moreover, the frequency vector (FV) is built to capture the structural information of textures. Finally, the concatenation of those SDMVs and FVs is used as a texture feature, and comprehensive experiments testify that our proposed method can get a satisfactory classification performance.

REFERENCES

[1] J. Ryu, S. Hong, and H. S. Yang, "Sorted consecutive local binary pattern for texture classification," *IEEE Trans. Image Process.*, vol. 24, no. 7, pp. 2254-2265, Jul. 2015.

[2] J. Ren, X. Jiang, and J. Yuan, "LBP encoding schemes jointly utilizing the information of current bit and other LBP bits," *IEEE Signal Process. Lett.*, vol. 22, no. 12, pp. 2373-2377, Dec. 2015.

[3] L. Liu, Y. Long, P. W. Fieguth, S. Lao, and G. Zhao, "BRINT: binary rotation invariant and noise tolerant texture classification," *IEEE Trans. Image Process.*, vol. 23, no. 7, PP. 3017-3084, Jul. 2014.

[4] X. Hong, G. Zhao, M. Pietikäinen, and X. Chen, "Combining LBP Difference and Feature Correlation for Texture Description," *IEEE Trans. Image Process.*, vol. 23, no. 6, pp. 2557-2568, Jun. 2014.

[5] M. Cote and A. B. Albu, "Robust texture classification by aggregating pixel-based LBP statistics," *IEEE Signal Process. Lett.*, vol. 22, no. 11, pp. 2102-2106, Nov. 2015.

[6] R. Davarzani, S. Mozaffari, and K. Yaghmaie, "Scale- and rotation-invariant texture description with improved local binary pattern features," *Signal Process.*, vol. 111, pp. 274-293, 2015.

[7] J. Feng, Y. Dong, L. Liang, and J. Pu, "Dominant-completed local binary pattern for texture classification," In Proc. *4th IEEE Int. Conf. Inf. Aut.*, Yunnan, China, Aug. 2015, pp. 233-238.

[8] J. F. Aujol, G. Aubert, and L. Blanc-Feraud, "Wavelet-based level set evolution for classification of textured images," *IEEE Trans. Image Process.*, vol. 12, no. 12, pp. 1634-1641, Dec. 2003.

[9] D. Charalampidis and T. Kasparis, "Wavelet-based rotational invariant roughness features for texture classification and segmentation," *IEEE Trans. Image Process.*, vol. 11, no. 8, pp. 825-837, Aug. 2002.

[10] G. Chen and B. Kégl, "Invariant pattern recognition using contourlets and AdaBoost," *Pattern Recognit.*, vol. 43, no. 3, pp. 579-583, 2010.

[11] Y. Qiao and L. Weng, "Hidden markov model based dynamic texture classification," *IEEE Signal Process. Lett.*, vol. 22, no. 4, pp. 509-512, Apr. 2015.

[12] S. C. Kim and T. J. Kang, "Texture classification and segmentation using wavelet packet frame and Gaussian mixure model," *Pattern Recognit.*, vol. 40, no. 4, pp. 1207-1221, 2007.

[13] S. Dua, U. R. Acharya, P. Chowriappa, and S. V. Sree, "Wavelet-based energy features for glaucomatous image classification," *IEEE Trans. Inf. Technol. Biomed.*, vol. 16, no. 1, pp. 80-87, Jan. 2012.

[14] T. Song, H. Li, F. Meng, Q. Wu, and B. Luo, "Exploring space-frequency co-occurrences via local quantized patterns for texture representation," *Pattern Recognit.*, vol. 48, no. 8, pp. 2621-2632, 2015.

[15] R. Davarzani, S. Mozaffari, and K. Yaghmaie, "Scale- and rotation-invariant texture description with improved local binary pattern features," *Signal Process.*, vol. 111, pp. 274-293, Jun. 2015.

[16] Z. Guo, L. Zhang and D. Zhang, "Rotation invariant texture classification using LBP variance (LBPV) with global matching," *Pattern Recognit.*, vol. 43, no. 3, pp. 706-719, Mar. 2010.

[17] S. R. Dubey, S. K. Singh, and R. K. Singh, "Local diagonal extrema pattern: a new and efficient feature descriptor for CT image retrieval," *IEEE Signal Process. Lett.*, vol. 22, no. 9, pp. 1215-1219, Sep. 2015.

[18] J. Zhang, J. Liang, and H. Zhao, "Local Energy Pattern for Texture Classification Using Self-Adaptive Quantization Thresholds," *IEEE Trans. Image Process.*, vol. 22, no. 1, pp. 31-42, Jan. 2013.

[19] T. Ojala, M. Pietikaninen, and T. Maenpaa, "Multiresolution gray-scale and rotion invariant texture classification with local bianry patterns," *IEEE Trans. Pattern Anal. Mach. Intell.*, vol. 24, no. 7, pp. 971-987, Jul. 2002.

[20] Z. Guo, L. Zhang, and D. Zhang, "A completed modeling of local binary pattern operator for texture classification," *IEEE Trans. Image Process.*, vol. 19, no. 6, pp. 1637-1663, Jun. 2010.

[21] X. Qi, R. Xiao, C. Li, Y. Qiao, J. Guo, and X. Tang, "Pairwise rotation invariant co-occurrence local binary pattern," *IEEE Trans. Pattern Anal. Mach. Intell.*, vol. 36, no. 11, pp. 2199-2213, Nov. 2014.

[22] Y. Dong and J. Ma, "Wavelet-based image texture classification using local energy histograms," *IEEE Signal Process. Lett.*, vol. 18, no. 4, pp. 247-250, Apr. 2011.

[23] Y. Dong, D. Tao, and X. Li, Nonnegative multiresolution representation based texture image classification, ACM Trans. Intell. Syst. and Technol., vol. 7, no. 1, pp. 4:1-4:21, 2015.

[24] H. Ji, X. Yang, H. Ling, and Y. Hu, "Wavelet domain multifractal analysis for static and dynamic texture classification," *IEEE Trans. Image Process.*, vol. 22, no. 1, pp. 286-299, Jan. 2013.

[25] S. Selvan and S. Ramakrishnan, "Texture classification using wavelet transformation," *IEEE Trans. Image Process.*, vol. 16, no. 11, pp. 2688-2696, Nov. 2007.

[26] Y. Dong, D. Tao, X. Li, J. Ma, and J. Pu, "Texture classification and retrieval using shearlets and linear regression," *IEEE Trans. Cybern.*, vol. 45, no. 3, pp. 358-369, Mar. 2015.

[27] Y. Dong and J. Ma, "Bayesian texture classification based on contourlet transform and BYY harmony learning of Poisson mixtures," *IEEE Trans. Image Process.*, vol. 21, no. 3, pp. 909-918, Mar. 2012.

[28] Y. Dong and J. Ma, "Feature extraction through contourlet subband clustering for texture classification," *Neurocomputing*, vol. 116, pp. 157-164, 2013.

[29] R. Eslami and H. Radha, "Translation-invariant contourlet transform and its application to image denoising," *IEEE Trans. Image Process.*, vol. 15, no. 11, pp. 3362-3374, Nov. 2006.

[30] X. Li, G. Cui, and Y. Dong, Graph regularized nonnegative low-rank matrix factorization for image clustering, IEEE Trans. Cybern., DOI:10.1109/TCYB.2016.2585355.